Computational model of fractal interface formation in bacterial biofilms

Caelan Brooks[1,2,3,4], Jake T. McCool[2,3,5], Alan Gillman[6¤], Gürol M. Süel[6], Andrew Mugler[7], Joseph W. Larkin[2,3,8*]

1 Department of Physical Sciences, Kutztown University of Pennsylvania, Kutztown, Pennsylvania, USA
2 Department of Physics, Boston University, Boston, Massachusetts, USA
3 Biological Design Center, Boston University, Boston, Massachusetts, USA
4 Department of Physics, Harvard University, Cambridge, Massachusetts, USA
5 Department of Physics, Cornell University, Ithaca, New York, USA
6 Division of Biological Sciences, University of California San Diego, La Jolla, California, USA
7 Department of Physics & Astronomy, University of Pittsburgh, Pittsburgh, Pennsylvania, USA
8 Department of Biology, Boston University, Boston, Massachusetts, USA

¤Current Address: Evident Scientific, Waltham, Massachusetts, USA
* jwlarkin@bu.edu

Abstract

Bacterial colonies benefit from cellular heterogeneity, with cells differentiating into diverse states of physiology and gene expression. As colonies grow, such cells in distinct states arrange into spatial patterns. To uncover the functional role of these emergent patterns, we must understand how they arise from cellular growth, phenotypic inheritance, and mechanical interactions among cells. Here we present a simple, agent-based model to predict patterns formed by motile and extracellular matrix-producing cells in developing populations of *Bacillus subtilis* bacteria. By incorporating phenotypic inheritance, differential mechanical interactions of the two cell types, and the escape of peripheral motile cells, our model predicts the emergence of a pattern: matrix cells surround a fractal-like population of interior motile cells. We find that, while some properties of the emergent motile-matrix interface depend on the initial spatial arrangement of cells, the distribution of motile cells at large radii are a product solely of the model's growth mechanism. Using a box-counting analysis, we find that the emergent motile-matrix interface exhibits a fractal dimension that increases as biofilms grow but eventually reaches a maximum as the thickness of the peripheral layer of matrix exceeds the capacity of the inner cells to push matrix cells out of the way. We find that the presence of the fractal interface correlates with a larger colony growth rate and increases the local proximity of motile and matrix cells, which could promote resource sharing. Our results show that simple computational models can account for morphological features of active systems like bacterial colonies, where colony-level phenotypes emerge from single cell-level properties and cells modifying their own environment.

Author summary

Like cells in our bodies, bacterial cells can differentiate into different cell types, which perform different roles in colonies. During the growth of *Bacillus subtilis* colonies, motile cells, which can swim, and matrix cells, which produce sticky polymers to adhere cells together, form reproducible spatial patterns. Multiple factors could drive the formation of these patterns, including inheritance of the motility and matrix states as cells divide, and different mechanical interactions between different cell types as they push each other around during growth. We created an agent-based computational model, in which we represent bacterial cells as occupying squares within a grid. We find that through inheritance of motile and matrix state and greater resistance to physical pushing by matrix cells, our model produces patterns similar to those observed in experiments—an exterior population of matrix cells surrounding an interior group of motile cells with fractal arms that branch into the outer matrix layer. Our results show that simple models can account for complex phenomena like the growth of heterogeneous bacterial colonies.

Introduction

In stressful environments, bacteria differentiate into heterogeneous states [1] of physiology [2] and gene expression [3]. For example, *Bacillus subtilis* bacteria generate multiple cell types characterized by distinct gene expression states [4]. These states include matrix producers, which synthesize extracellular polymers to bind cells together into biofilms [5] and motile cells, which exhibit swimming and swarming behavior [6]. As cells differentiate into these states, they change how they interact with each other and the environment [7, 8]. The contents of surface-adhered biofilm colonies contain cells in numerous phenotypic states [9, 10], leading microbiologists to make analogies between the growth of biofilms and cell differentiation during development of multicellular organisms [11–13].

Bacterial biofilms are defined by the synthesis of extracellular matrix, which attaches cells to surfaces and to each other [14]. In *B. subtilis*, the matrix-production and motile states are regulated by a transcription factor network whose interactions cause the two phenotypes to be mutually exclusive [6, 15] and heritable [16]. Within *B. subtilis* biofilms, these phenotypic states form repeatable spatiotemporal patterns [10, 17]. Despite the robustness of these patterns, their functional relevance remains unclear. To explore the functional role of spatiotemporal patterns in bacterial colonies, we must understand how they arise, and so it is essential to develop models that predict patterns based on biological and physical factors that may create them. These factors include phenotypic inheritance in dividing cells [1] and mechanical interactions among bacteria [18].

Agent-based models provide a framework to ask how colony-scale phenomena emerge from the properties of individual bacterial cells. Such simulations have been used to show how mechanical interactions lead to cellular re-ordering in dense colonies [19], how cell shape affects the spatial partitioning of different species within microbial communities [20], and how mechanical interactions and cell shape together lead to fractal patterning in bacterial layers [21]. Furthermore, agent-based simulations have been used to account for feedback of mechanical interactions on cell growth [22] and interplay of mechanics with with other forms of interaction like quorum sensing [23]. Nevertheless, the combined effects of mechanical interactions and heritable phenotypic differences, including different degrees of motility, remain poorly understood.

Here, we present a simple, agent-based, computational model of motile-matrix pattern formation in growing populations of *B. subtilis* and compare our results to

experimental data. The model takes into account three key factors in the development of motile-matrix patterning. First, cells are either motile or matrix, with daughter cells perfectly inheriting their parent's phenotype. Second, motile cells exposed to the edge of the colony will "disperse" and swim away. Third, when a cell on the colony interior divides, it must shove other cells out of the way to make space for the new cell. Matrix cells resist shoving more strongly than motile cells. With these three rules, our model lets a biofilm grow from an initial inoculum of cells. The model produces a biofilm with an interior population of motile cells surrounded by matrix cells. The interface between these two populations develops a fractal edge. We characterize the predicted pattern by computing the fractal dimension of this interface and compare it to experimental data from a *B. subtilis* biofilm grown in a microfluidic device [24]. Our model shows how single cell-level properties, coupled with cells modifying the local environment, can lead to population-level phenomena.

Results

Emergence of motile-matrix patterns in *B. subtilis* biofilms

To observe the formation of motile-matrix patterns, we grew *B. subtilis* biofilms in a microfluidic device confined to a thickness of 1-3 cell layers (Fig. 1) [24]. We used a strain with separate transcriptional fluorescent reporters for promoters of motility genes and matrix production genes [10]. Two key observations emerged from this experiment. First, upon initial cell loading, colonies did not exhibit distinguishable patterns of motile or matrix cells. Second, after approximately 16 hours of growth, biofilms had organized into a distinctive pattern, with a fractal-like population of motile cells surrounded by matrix-producing cells (Fig. 1).

From our observations, two questions arose. 1) How, if at all, does the initial arrangement of motile and matrix cells influence that pattern that arises during growth? 2) What mechanism leads to such a pattern? We sought to create a computational model that could answer these questions.

An agent-based, mechanistic cell growth model

We model the dynamics of biofilm growth using sites on a square lattice (Fig. 2). For computational simplicity, we restrict ourselves to parameters for which patterns freeze when our simulated biofilms reach thousands of sites, whereas our experimental biofilms typically grow to hundreds of thousands of cells. Therefore, each site can be thought of as a coarse-grained packet of cells of the same phenotype (motile or matrix). Furthermore, as described below, we assume no preferential direction for site growth apart from steric hinderance due to existing sites (although we later check for the effects of preferential growth direction). This assumption is also consistent with sites being packets of cells, given that the packets are larger than the lengthscale over which cells align due to their rod-like shape. We will later account for this coarse-graining when comparing to the experimental data. From here on we use 'sites' and 'cells' interchangeably, both referring to a lattice site within the grid.

We initiate the system by creating an inoculum of cells containing both phenotypes. Each cell is given a growth time that acts as an internal clock, indicating when it is time for the cell to divide (Fig. 2A). These growth times are randomly drawn from a normal distribution centered at 1, with a standard deviation of 0.1. Thus time is rescaled by the mean doubling time for a cell (or packet of cells).

At each step of the simulation, the cell with the minimum growth time is chosen (Fig. 2B). The chosen cell then goes through a process of determining if and how to divide

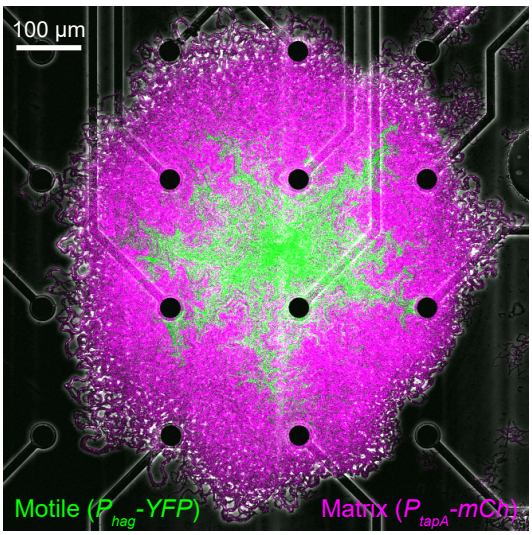

Fig 1. Phenotypic Patterning in a Bacterial Biofilm. Fluorescence image of a *Bacillus subtilis* biofilm grown in a microfluidic device. False color green is the signal from a reporter on motility genes ($P_{hag} - YFP$). Magenta is the signal from a matrix production reporter ($P_{tapA} - mCherry$).

and produce a daughter cell. If the cell is on the edge of the biofilm, it will choose from the neighboring empty spaces with equal probability and grow into one of them, filling the space with a daughter cell. Daughter cells inherit their mother's phenotype with no switching. The two new cells will then be assigned random growth times.

If instead the dividing cell is surrounded by other cells (Fig. 2C), then it must shove those cells out of the way to create space for a new cell (Fig. 2D). The direction of growth is chosen with an equal probability of being up, down, left, or right. We then compute the total biomass between the chosen cell and the edge of the growing colony in the chosen direction (Fig. 2D). We represent biomass with two random variables, α and β, corresponding to motile and matrix cells respectively. These variables are normally distributed with $\langle\beta\rangle > \langle\alpha\rangle$. Here we use $\alpha = 1$ and $\beta = 2$, and a standard deviation of 0.1 for both distributions. Because matrix cells have greater biomass in our model, they offer more resistance to pushing by growing cells. This choice reflects the fact that matrix cells produce polymers that adhere them to the substrate and to each other.

We further assume there is a mechanical constraint on how much biomass a cell can shove in order to create the space to produce a daughter cell: if too much biomass must be moved to create room for a new cell, then a chosen cell will not grow, and will be assigned a new growth time. We represent the mechanical constraint with a parameter called the shoving capacity, C_{sh}. If the bounding biomass is less than or equal to C_{sh}, then the stack of cells will be pushed out of the way, and a new daughter cell will be created (Fig. 2E). The original growing cell and the new cell will then be given new growth times (Fig. 2F) and the simulation will progress by choosing the cell with the next minimum growth time.

Finally, if at any step of the simulation there is a motile cell at the edge of the biofilm, it will disperse and be removed from the colony, which is a reasonable assumption based on previous observation of passive escape of motile cells from the edges of biofilms [25].

Simulating biofilm growth from a small group of initial cells, our model produces colonies with motile-matrix patterns qualitatively similar to those from experiments

(Fig. 2G). We find shoving capacities within the range of $C_{sh} = 12 - 18$ produce fractal structures most like those observed in experiments. With extreme values exhibiting more circular like shapes. In our model, the interior pattern of motile cells eventually becomes frozen in place after the width of exterior matrix cells exceeds the shoving capacity.

Two key assumptions of our model reproduce salient aspects of the motile matrix pattern: (1) dispersion of peripheral motile cells creates a motile interior surrounded by a matrix exterior, and (2) differential resistance of the two phenotypes moves motile cells during growth, creating branched arms. After observing similar patterns to those in the experiment, we wanted to know how the initial arrangement cells influenced the final pattern.

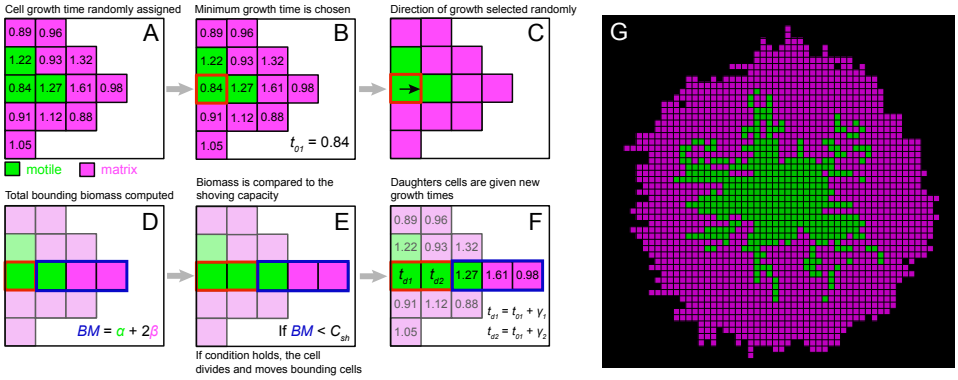

Fig 2. Agent-Based Growth Model. (A-F) Growth and displacement mechanism. (A) Growth times are drawn from a Gaussian distribution and are assigned to each site. (B) The lattice site with the minimum growth time (outlined in red here) is selected and given the opportunity to grow, where t_{01} is the initial growth time. (C) The direction of growth is chosen randomly from four options. (D) If the cell is not on the edge, the total biomass (BM) will be measured in the growth direction. The biomass of each cell type is represented by α and β, which are Gaussian-distributed with different means ($\langle\beta\rangle > \langle\alpha\rangle$). (E) The biomass is pushed under the condition $BM < C_{sh}$ (F) New sites are given growth times based on t_{01}. (G) Resulting pattern once interior motile cells become frozen because biomass exceeds shoving capacity.

Dependence of phenotypic patterns on initial conditions

To investigate how our model's predictions depend on the initial arrangement of motile and matrix cells, we carried out simulations with three different initial conditions (Fig. 3). In the first case, termed "bullseye," a layer of matrix cells surrounds a group of motile cells in the initial inoculum (Fig. 3A). In the second condition, "mixed," the initial colony consists of a mixture of motile and matrix cells, with each initially occupied lattice site having equal probability of being either type (Fig. 3B). The third condition, "concentric," consists of alternating rings of each cell type with matrix cells residing on the outermost ring. We show examples of our model's simulated biofilm growth from these three conditions in Fig. 3A, B, and C.

Each starting condition appears to create a different final pattern (Fig. 3A, B, and C right). However, we observe that, in the final state for each condition, the regions of the colonies that were populated only by the growth dynamics of the model, and not by the initial cells, exhibit patterns that are qualitatively similar: branches of motile cells that penetrate into an outer layer of matrix-producing cells. We highlight this in Fig.

3D, E, F. When the initial group of cells is visually excluded, the ability to distinguish which final pattern results from each distinct initial condition is lost.

We next sought to quantify the final patterns of motile and matrix cells generated from each initial condition. We observed that every pattern simulated by our model featured motile cells in the interior surrounded by matrix cells. To quantify these patterns, we computed, for a given ring of cells, the motile cell proportion as a function of the distance of the ring from the colony center. In Fig. 3G, we plot such curves for bullseye, mixed, and concentric conditions. Each curve is an average of 300 simulations run under the same conditions. Within each initial condition, we analyzed three different initial colony radii. The initial proportion of motile cells was kept roughly constant for each initial condition when the inoculation radius changed. All cases feature patterns where the fraction of motile cells is high in the center and decays near the edge. However, the curves differ in key ways. For different initial conditions, the fraction of motile cells drops off at different distances from the colony center. The same is true for the case of different initial radii within the same initial condition subset: larger initial colonies exhibit a larger radius at which the motile proportion drastically decreases (3G).

Motivated by our observation in Fig. 3D, E, F that biofilm regions that were populated only by model growth looked the same, we thought that perhaps the curves of Fig. 3G would collapse if the initial conditions were taken into account in the proper way. When we normalized the proportion of motile cells throughout different radii by the initial number of motile cells, we produced the curves in Fig. 3H. In this case, we observe a collapse not only of all curves within an initial condition subset, but also of curves representing all initial conditions. The point of collapse of Fig. 3H represents the radius below which the initial condition has an effect. Beyond this point, all normalized curves collapse, illustrating that our model simulates the distribution of motile cells within biofilms during growth in a way that is insensitive to the initial cell arrangement. This result suggests that the growth dynamics of our model produce patterns of motile and matrix cells that are robust to changes in the initial cell arrangement.

Fractal interface formation between cell types

In both experimental images and model output, the interface between matrix cells and motile cells appeared to have a fractal character (Fig. 1, Fig. 2G). For this reason, we chose to quantify the patterns predicted by our model with fractal dimension (Fig. 4A,B). At each time point for model biofilms, we found the outline of the motile-matrix interface and computed its fractal dimension using box-counting [26]. In this technique, the number of pixels containing a part of the interface is counted. Space is then divided into larger and larger boxes and, for each box size, the number of occupied boxes is counted (Fig. 4A). The number of occupied boxes scales with some power of the box size depending on the shape of the interface. That exponent is the fractal dimension. It is 1 for a simple line, 2 for a two-dimensional plane, and between 1 and 2 for a rough interface like that in our model. To extract the fractal dimension for the interface in our model, we plotted the box size and the number of occupied boxes on a log-log plot and fit a regression line. The negative slope of the regression line is the fractal dimension, D (Fig. 4B).

For simulated biofilms initialized with a bullseye pattern, the fractal dimension starts out near 1 as the motile-matrix interface is smooth for this condition. Once we begin simulating growth with the model, cells shove each other out of the way as they grow, roughening the interface, and increasing the fractal dimension. However, once the outer matrix layer thickness exceeds the shoving capacity, the motile-matrix interface freezes into place and the fractal dimension saturates (Fig. S1). Because increasing the shoving capacity increases the time during which cells can grow and push each other

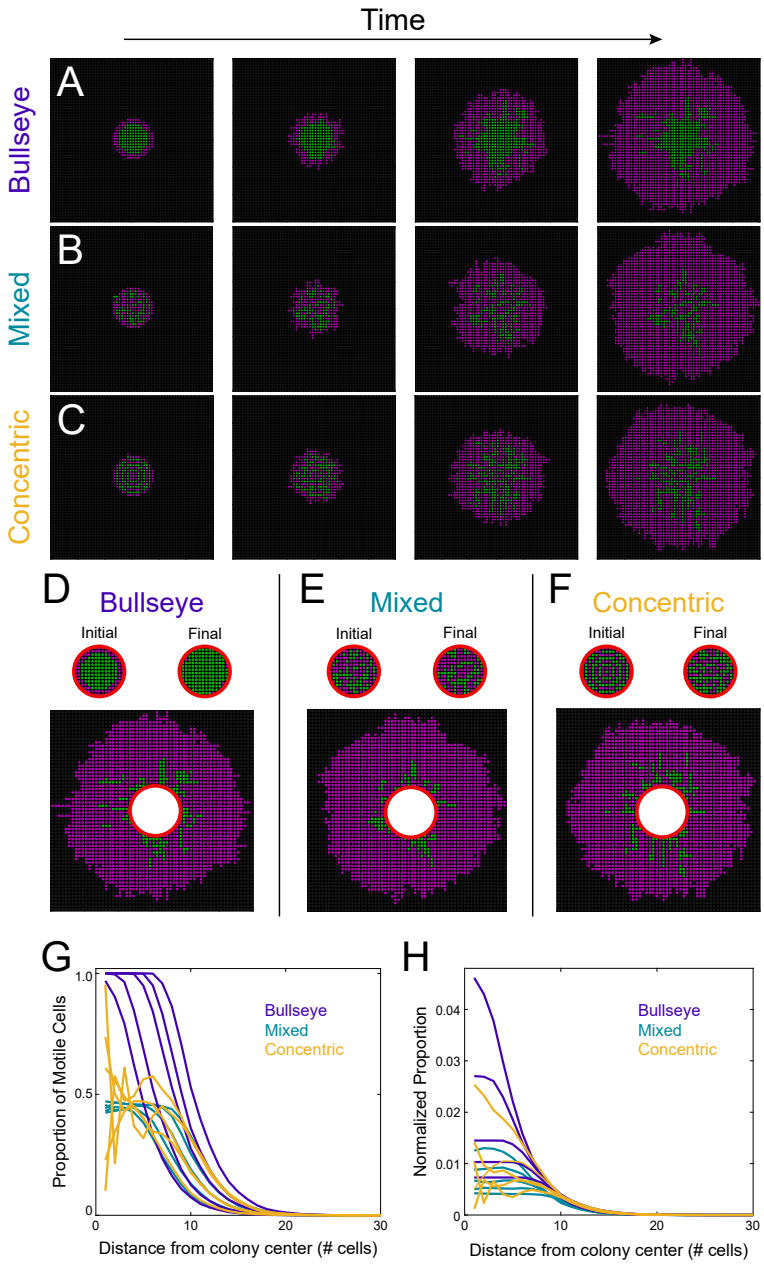

Fig 3. Dependence of Patterns on Initial Conditions. The evolution of the system from three different initial conditions: (A) bullseye, (B) mixed, and (C) concentric. (D-F) Visual isolation of region of the biofilm unaffected by the initial condition. (G) Proportion of motile cells within a ring at a particular distance from the center of the final pattern, as a function of the distance. Each line within an initial condition subset represents a different initial radius value ranging from $R_0 = 4$ to $R_0 = 8$ (larger initial radii correspond to falloffs farther from the center). (H) When the proportion of motile cells is divided by the initial number of motile cells, a collapse is observed beyond a distance from the center corresponding to the initial condition.

around, we hypothesized that the saturating fractal dimension would increase with shoving capacity. After simulating biofilm growth for a range of shoving capacities, we found that saturating fractal dimension does indeed increase with shoving capacity (Fig. 4C). The behavior of the fractal dimension in Fig. 4C is robust to changes in cell growth decisions, for example whether the direction of cell growth is random or preferential to the previous growth direction chosen by the parent cell (Fig. S2).

We wanted to know how the fractal dimension of experimental biofilms compared to that of the model. To determine the experimental fractal dimension, we thresholded biofilm images, found the outline of the interior motile population, and performed box-counting. To account for the fact that a lattice site corresponds to a coarse-grained packet of cells, we down-sampled our experimental images to make them the same resolution as the model (Fig. 4D). We found that the experimental fractal dimension was 1.26 ± 0.03 ($N = 4$), which is consistent with the range predicted by the model (Fig. 4D).

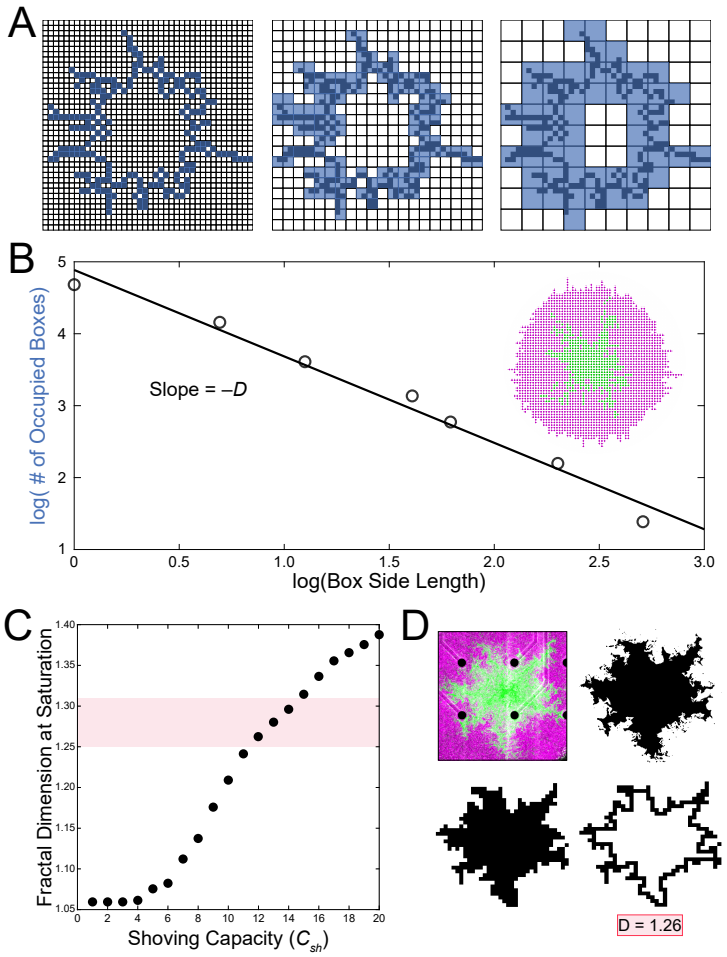

Fig 4. Fractal Dimension of Phenotype Interface. Fractal dimension is found using the box counting method: (A) Grids of different box sizes are fit to the internal motile sub-population to produce a graph like (B). The negative of the slope is the fractal dimension. (C) The fractal dimension at saturation increases with the shoving capacity. (D) Fractal dimension analysis of experimental biofilms. Fractal dimension corresponds to shaded region in C.

Potential biological implications of a fractal interface

Our model gives us the opportunity to ask how specific motile-matrix patterns may impart function to biofilms. We hypothesized that formation of a fractal interface may allow colonies to expand faster and to maximize the physical contact between motile and matrix cells. The latter factor may be important if the two cell types share a public good such as matrix polymers.

To investigate the question of colony expansion rate, we simulated the growth of biofilms with a range of shoving capacities C_{sh}, and therefore a range of resulting fractal dimensions (Fig. 4C). For each value of C_{sh}, we computed the average colony radius at each time point and extracted the mean expansion rate (Fig. 5A). We found that expansion rate increased with saturating fractal dimension, suggesting that colonies expand faster into new areas if they form rougher interfaces.

To investigate the question of how fractal dimension impacts the average distance between matrix cells and their nearest motile cells, we simulated growth under conditions that lead to two different fractal dimensions. We then computed the distance to the nearest motile cell for every matrix cell after the simulated colony reached a saturating fractal dimension. We plot a histogram of these distances in Fig. 5B. For a biofilm with a smooth motile-matrix interface ($C_{sh} = 0$ and $D = 1.068$), we observe a broad range of nearest-motile-neighbor distances, with a large portion of the matrix population being more than three sites away from a motile cell (gray). On the other hand, for a biofilm with a fractal interface ($C_{sh} = 17$ and $D = 1.361$), we find that a large fraction of matrix cells lie within a few sites of its nearest motile neighbor (black).

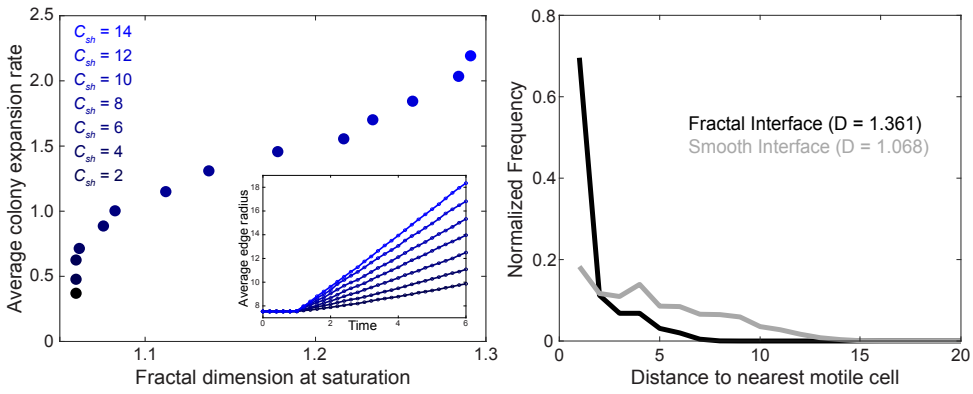

Fig 5. Potential Functional Relevance of a Fractal Interface. (A) Average colony expansion rate as a function of the fractal dimension at saturation. Colors indicate different shoving capacities. The inset shows how the rate of colony expansion is found from the change in average radius over time. (B) Distribution of the distance to the nearest matrix cell for motile cells for a fractal interface (black) or a smooth interface (gray).

Discussion

We have presented a simple, agent-based model that accounts for multiple features of patterns formed by motile and matrix cell phenotypes in *B. subtilis* colonies. Specifically, the model addresses two key questions: 1) how do motile-matrix patterns depend on initial conditions? 2) What mechanism leads to the experimentally observed

pattern? On the first question, we find that in uncolonized regions of space, our model's dynamics create patterns of motile cells that are robust to the initial arrangement of cells. This arises from the model spatially distributing cells not only through growth and inheritance, but also by mechanical shoving during cell replication. For three different starting arrangements, we found that the limiting pattern depended strongly on the initial condition within the initial inoculum radius, but beyond that radius the normalized density of motile cells collapsed for all three initial patterns. On the second question, the model predicts the emergence of a fractal interface between the two cell types within a biofilm with fractal dimension consistent with experimental observations. Simulated colonies with higher fractal dimension exhibit faster expansion and closer physical distance between motile and matrix cells, suggesting potential functional roles for this pattern-formation process. The latter phenomenon may be advantageous for sharing of public goods between the two cell types.

Our model greatly simplifies *B. subtilis* colony growth. Among other things, the model does not take into account nutrient availability, phenotypic switching, cell shape, or the fact that cells grow continuously and not in discrete time. However, despite these simplifications, it makes predictions that are consistent with experimental data and suggests a mechanical mechanism for the spatial distribution of phenotypes within biofilms. Furthermore, our model establishes a starting point for more detailed agent-based simulations that take into account other factors like active cell movement, metabolism, or cell shape.

The agent-based model is sufficiently minimal that future studies may investigate its relationship to continuum expansion models. The expansion of a less viscous fluid into a more viscous one is known to lead to branching or fingering patterns [27–30] reminiscent of the ones we observe here. Indeed, viscous fingering is thought to underlie aspects of pattern formation in microbial systems [31, 32]. It is an interesting open question whether taking the continuum limit of our lattice update rules would recover a known continuity equation from fluid mechanics, or a variant thereof. Such an extension has the potential to generalize the mechanism we report here beyond the realm of microbial communities, or beyond living systems entirely.

Our finding that the final pattern only depends on the initial conditions at low radii, and beyond this the resulting pattern is mechanistically determined, is something that we could not have found from the experiment. The reason is that there is significant uncertainty in our ability to determine the differentiation state at early time points. This is one advantage to mechanistic modeling: it allows one to validate experiments in particular regimes, and in doing so, makes predictions for regimes not yet accessible.

Attempts to use agent-based or statistical physics models for living systems must take into account an essential feature of cells and organisms: they not only sense their environment, they also change it. This feedback can lead to remarkable phenomena that collectives of cells can take advantage of. Our results capture this phenomenon in a simple way. As biofilm cells grow, they create a mechanically constrained environment, altering patterns of growth and leading to a wide variety of potential cell-type patterns.

Materials and methods

Model

Determining the Fractal Dimension of Model Output

The fractal dimension is found using the box counting method. Within the model, first the internal shape is recognized through a recursive shape fill method. From this, the perimeter of this shape is isolated and the box counting method enforced. In order to correctly identify the dimension of the shape, the grids of different box sizes are fit to

the perimeter identified. This that, as the biofilm grows, the dimensions of the grids utilized in analysis will change as well. At each time step, we produce a graph of ln(box size) vs ln(occupied boxes). The negative slope of a regression line is taken as the fractal dimension of the internal motile sub-population. The number of points within this plot is reflective of the number of grids of different box sizes fit to the perimeter. The algorithm attempts to maximize the number of points while limiting the overall dimension of the grid used to cover the internal shape. When repeated over numerous time steps as the biofilm grows and then averaging over hundreds of systems, we are able to produce the results shown in Fig. 4.

Experiment

We grew biofilms in a microfluidic device as described in [24]. Biofilm growth media consisted of liquid MSgg medium containing 5 mM potassium phosphate buffer (pH 7.0), 100 mM MOPS buffer (pH 7.0, adjusted using NaOH), 2 mM $MgCl_2$, 700 µM $CaCl_2$, 5 µM $MnCl_2$, 100 µM $FeCl_3$, 1 µM $ZnCl_2$, 2 µM thiamine HCl, 0.1 mM sodium citrate, 0.5. % (v/v) glycerol and 0.4% (w/v) monosodium glutamate. Media were made from stock solutions immediately before experiments, and the stock solution of glutamate made fresh daily. We acquired images with a Fluoview FV3000 scanning confocal microscope (Olympus Corp.) using a 10X, 0.3 NA air objective. We performed experiments with a modified *B. subtilis* NCIB3610 strain with Venus yellow fluorescent protein (YFP) fused to the *hag* promoter and mCherry fused to the *tapA* promoter.

Data Analysis

We analyzed images in Fiji [33]. In order to accurately compare our model to our experimental data, we first needed to coarse-grain the experimental images–ensuring that the experimental pixel size was comparable to the cell size of our model. To achieve accurate scaling, we first cropped the time-lapse tiff stack for the YFP channel so the saturated fractal filled the entire frame. At this point, select frames were analyzed individually and were only chosen after a clear bimodal distribution arose in the YFP channel–the brighter peak representing the high concentration of motile cells inside the motile/matrix interface and the dimmer peak representing regions of the biofilm containing mostly matrix cells. This step ensured that there was minimal bias in thresholding, as images were thresholded simply by selecting the brighter peak of inner motile cells. After filling the holes of the thresholded image, we could resize the entire frame to 40 by 40 pixels, so it was comparable to the size of the saturated fractal in the computer model. Next, we converted the threshold to binary and the fractal was cropped to fit the entire frame–this ensures a more accurate measure of its fractal dimension. We could finally outline the interface and use Fiji's fractal box count tool, selecting the same sized boxes used for the computer model's fractal analysis, to identify the fractal dimension of the experimental interface.

Supporting information

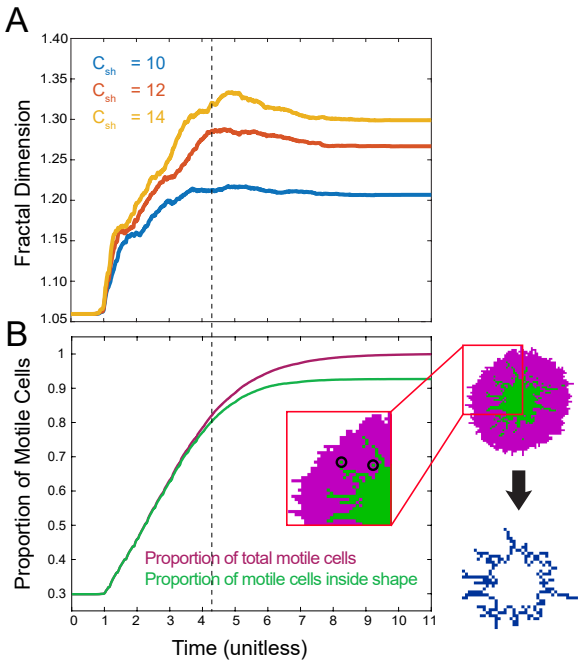

Fig S1. Dynamics of Fractal Dimension. (A) The evolution of the fractal dimension as the simulated biofilm grows (300 simulations averaged). Each line represents biofilm growth under a different shoving capacity. (B) The peak and then decline in fractal dimension is credited to the formation of motile islands. These are motile cells that are not connected to the internal motile shape, but remain stuck inside the matrix producing cells. The split in the two curves signalling the formation of these islands coincides with the peak of the fractal dimension curve ($C_{sh} = 12$ used).

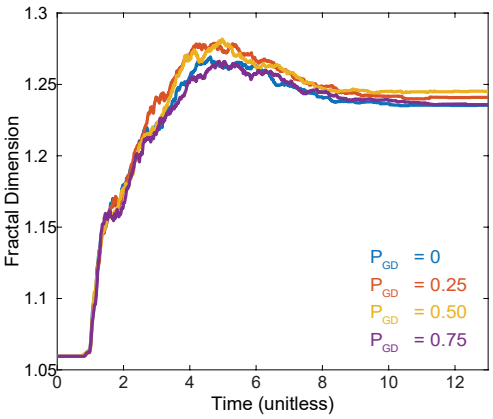

Fig S2. Effects of Preferential Growth Direction. Each line represents a condition in which each cell has a certain probability of growing in the same direction that it previously grew into. The probability for a lineage to continue to choose the same growth direction does not effect how the fractal dimension of the internal motile shape evolves.

Acknowledgments

This work was supported by the Burroughs Wellcome Fund (Career Award at the Scientific Interface, J.W.L.), the National Science Foundation (Grant No. 2027108, J.W.L.; Grant No. 1852266, C.B.; Grant No. PHY1945018, A.M.), the National Institute of General Medical Sciences (Grant No. 1R35GM142584-01, J.W.L.; Grant Nos. R01 GM121888 and R35 GM139645, G.M.S.), the Simons Foundation (Award No. 376198, A.M.), the Defense Advanced Research Projects Agency (Grant No. HR0011-16-2-0035, G.M.S.) and the Howard Hughes Medical Institute (Simons Foundation Faculty Scholar Award, G.M.S.).

We acknowledge members of the Larkin Lab, Neil Marya, and Patrick Powers for comments on the paper.

Author Contributions

Conceptualization: CB, AM, JWL. Formal Analysis: CB, JTM. Funding Acquisition: AM, GMS, JWL. Investigation: AG. Supervision: AM, JWL. Visualization: CB, AM, JWL. Writing – Original Draft Preparation: CB, JTM, AM, JWL. Writing – Review & Editing: GMS, CB, JTM, AM, JWL.

References

1. Veening JW, Smits WK, Kuipers OP. Bistability, Epigenetics, and Bet-Hedging in Bacteria. Annual Review of Microbiology. 2008;62(1):193–210. doi:10.1146/annurev.micro.62.081307.163002.

2. Nikolic N, Schreiber F, Dal Co A, Kiviet DJ, Bergmiller T, Littmann S, et al. Cell-to-cell variation and specialization in sugar metabolism in clonal bacterial populations. PLOS Genetics. 2017;13(12):1–24. doi:10.1371/journal.pgen.1007122.

3. Maamar H, Raj A, Dubnau D. Noise in Gene Expression Determines Cell Fate in *Bacillus subtilis*. Science. 2007;317(5837):526–529. doi:10.1126/science.1140818.

4. Lopez D, Vlamakis H, Kolter R. Generation of multiple cell types in *Bacillus subtilis*. FEMS Microbiology Reviews. 2008;33(1):152–163. doi:10.1111/j.1574-6976.2008.00148.x.

5. Vlamakis H, Chai Y, Beauregard P, Losick R, Kolter R. Sticking together: building a biofilm the *Bacillus subtilis* way. Nature Reviews Microbiology. 2013;11(3):157–168. doi:10.1038/nrmicro2960.

6. Kearns DB, Losick R. Cell population heterogeneity during growth of *Bacillus subtilis*. Genes & Development. 2005;19(24):3083–3094. doi:10.1101/gad.1373905.

7. Armbruster CR, Lee CK, Parker-Gilham J, de Anda J, Xia A, Zhao K, et al. Heterogeneity in surface sensing suggests a division of labor in *Pseudomonas aeruginosa* populations. eLife. 2021;8:e45084. doi:10.7554/eLife.45084.

8. Steinberg N, Keren-Paz A, Hou Q, Doron S, Yanuka-Golub K, Olender T, et al. The extracellular matrix protein TasA is a developmental cue that maintains a motile subpopulation within *Bacillus subtilis* biofilms. Science Signaling. 2020;13(632). doi:10.1126/scisignal.aaw8905.

9. Stewart PS, Franklin MJ. Physiological heterogeneity in biofilms. Nature Reviews Microbiology. 2008;6(3):199–210. doi:10.1038/nrmicro1838.

10. Vlamakis H, Aguilar C, Losick R, Kolter R. Control of cell fate by the formation of an architecturally complex bacterial community. Genes & Development. 2008;22(7):945–953. doi:10.1101/gad.1645008.

11. O'Toole G, Kaplan HB, Kolter R. Biofilm Formation as Microbial Development. Annual Review of Microbiology. 2000;54(1):49–79. doi:10.1146/annurev.micro.54.1.49.

12. Stoodley P, Sauer K, Davies DG, Costerton JW. Biofilms as Complex Differentiated Communities. Annual Review of Microbiology. 2002;56(1):187–209. doi:10.1146/annurev.micro.56.012302.160705.

13. Rosenberg SM. Life, Death, Differentiation, and the Multicellularity of Bacteria. PLOS Genetics. 2009;5(3):1–3. doi:10.1371/journal.pgen.1000418.

14. Flemming HC, Wingender J. The biofilm matrix. Nature Reviews Microbiology. 2010;8(9):623–633. doi:10.1038/nrmicro2415.

15. Chai Y, Norman T, Kolter R, Losick R. An epigenetic switch governing daughter cell separation in *Bacillus subtilis*. Genes & Development. 2010;24(8):754–765. doi:10.1101/gad.1915010.

16. Norman TM, Lord ND, Paulsson J, Losick R. Memory and modularity in cell-fate decision making. Nature. 2013;503(7477):481–486. doi:10.1038/nature12804.

17. Srinivasan S, Vladescu ID, Koehler SA, Wang X, Mani M, Rubinstein SM. Matrix Production and Sporulation in *Bacillus subtilis* Biofilms Localize to Propagating Wave Fronts. Biophysical Journal. 2018;114(6):1490–1498. doi:https://doi.org/10.1016/j.bpj.2018.02.002.

18. Persat A, Nadell CD, Kim MK, Ingremeau F, Siryaporn A, Drescher K, et al. The Mechanical World of Bacteria. Cell. 2015;161(5):988–997. doi:10.1016/j.cell.2015.05.005.

19. Volfson D, Cookson S, Hasty J, Tsimring LS. Biomechanical ordering of dense cell populations. Proceedings of the National Academy of Sciences. 2008;105(40):15346–15351. doi:10.1073/pnas.0706805105.

20. Smith WPJ, Davit Y, Osborne JM, Kim W, Foster KR, Pitt-Francis JM. Cell morphology drives spatial patterning in microbial communities. Proceedings of the National Academy of Sciences. 2017;114(3):E280–E286. doi:10.1073/pnas.1613007114.

21. Rudge TJ, Federici F, Steiner PJ, Kan A, Haseloff J. Cell polarity-driven instability generates self-organized, fractal patterning of cell layers. ACS synthetic biology. 2013;2(12):705–714.

22. Winkle JJ, Igoshin OA, Bennett MR, Josić K, Ott W. Modeling mechanical interactions in growing populations of rod-shaped bacteria. Physical biology. 2017;14(5):055001.

23. Narla AV, Borenstein DB, Wingreen NS. A biophysical limit for quorum sensing in biofilms. Proceedings of the National Academy of Sciences. 2021;118(21).

24. Comerci CJ, Gillman AL, Galera-Laporta L, Gutierrez E, Groisman A, Larkin JW, et al. Localized electrical stimulation triggers cell-type-specific proliferation in biofilms. Cell Systems. 2022;doi:https://doi.org/10.1016/j.cels.2022.04.001.

25. Stoodley P, Wilson S, Hall-Stoodley L, Boyle JD, Lappin-Scott HM, Costerton JW. Growth and Detachment of Cell Clusters from Mature Mixed-Species Biofilms. Applied and Environmental Microbiology. 2001;67(12):5608–5613. doi:10.1128/AEM.67.12.5608-5613.2001.

26. Gagnepain JJ, Roques-Carmes C. Fractal approach to two-dimensional and three-dimensional surface roughness. Wear. 1986;109(1):119–126. doi:https://doi.org/10.1016/0043-1648(86)90257-7.

27. Saffman PG, Taylor GI. The penetration of a fluid into a porous medium or Hele-Shaw cell containing a more viscous liquid. Proceedings of the Royal Society of London Series A Mathematical and Physical Sciences. 1958;245(1242):312–329.

28. Bensimon D, Kadanoff LP, Liang S, Shraiman BI, Tang C. Viscous flows in two dimensions. Reviews of Modern Physics. 1986;58(4):977.

29. Homsy GM. Viscous fingering in porous media. Annual review of fluid mechanics. 1987;19(1):271–311.

30. Paterson L. Radial fingering in a Hele Shaw cell. Journal of Fluid Mechanics. 1981;113:513–529.

31. Ben-Jacob E, Cohen I, Levine H. Cooperative self-organization of microorganisms. Advances in Physics. 2000;49(4):395–554.

32. Klapper I, Dockery J. Finger formation in biofilm layers. SIAM Journal on Applied Mathematics. 2002;62(3):853–869.

33. Schindelin J, Arganda-Carreras I, Frise E, Kaynig V, Longair M, Pietzsch T, et al. Fiji: an open-source platform for biological-image analysis. Nature Methods. 2012;9(7):676–682. doi:10.1038/nmeth.2019.